Exact Matrix Product States for Quantum Hall Wave Functions

Michael P. Zaletel[1] and Roger S. K. Mong[1, 2]

[1]*Department of Physics, University of California, Berkeley, California 94720, USA*
[2]*Department of Physics, California Institute of Technology, Pasadena, California 91125, USA*

We show that the model wave functions used to describe the fractional quantum Hall effect have exact representations as matrix product states (MPS). These MPS can be implemented numerically in the orbital basis of both finite and infinite cylinders, which provides an efficient way of calculating arbitrary observables. We extend this approach to the charged excitations and numerically compute their Berry phases. Finally, we present an algorithm for numerically computing the real-space entanglement spectrum starting from an arbitrary orbital basis MPS, which allows us to study the scaling properties of the real-space entanglement spectra on infinite cylinders. The real-space entanglement spectrum obeys a scaling form dictated by the edge conformal field theory, allowing us to accurately extract the two entanglement velocities of the Moore-Read state. In contrast, the orbital space spectrum is observed to scale according to a complex set of power laws that rule out a similar collapse.

I. INTRODUCTION

The fractional quantum Hall (FQH) effects are exotic phases of matter that appear when interacting 2D systems are subject to large magnetic fields. They are the foremost example of *topologically ordered* phases, which are characterized by their pattern of long range entanglement rather than by local order parameters.[1] In addition to signatures such as gapless edge excitations, fractional statistics, and topological ground state degeneracy, recently ideas originating from quantum information, such as the entanglement spectrum, have become important tools for describing the topological order of these states.[2–4]

Given a bipartition of the system into two sub-Hilbert spaces, $\mathfrak{H} = \mathfrak{H}_A \otimes \mathfrak{H}_B$, we can decompose any wave function $|\Psi\rangle$ in terms of wave functions which live solely in A or B:

$$|\Psi\rangle = \sum_a e^{-\frac{1}{2}E_a}|\Psi_a^A\rangle \otimes |\Psi_a^B\rangle, \qquad (1)$$

with the restriction that the 'entanglement spectrum' E_a is real and that the 'Schmidt vectors' $|\Psi_a^A\rangle$'s form an orthonormal set (as do $|\Psi_a^B\rangle$'s). It was argued,[2] and later numerically verified,[5] that when A, B are chosen to be regions in space, the entanglement spectrum of the FQH states are closely related to the conformal field theory (CFT) describing their gapless edge excitations.[6] In fact, for the 'model' wave functions such as the Laughlin[7] and Moore-Read (MR) states,[8] the states of the Schmidt spectrum are in *exact* correspondence with the states of the associated CFT.

A second realm in which entanglement has come to play an important role is for a set of variational wave functions called 'matrix products states' (MPS)[9] in one-dimension (1D) or 'tensor networks'[10] in higher dimensions. These are the variational states of the highly successful density matrix renormalization group (DMRG) method,[11,12] which succeeds because MPS efficiently capture the structure of entanglement in many body wave functions.[13] The precise relationship between topological order and tensor network representations is a subject of ongoing work, but in 1D at least a complete classification of symmetry protected topological (SPT) order for both gapped 1D spin and fermion chains was recently accomplished using the MPS representation of the ground state.[14–17] Given a set of sites labeled by i, each with local basis $|m_i\rangle$, an MPS $|\psi\rangle$ is defined by a set of 'B-matrices',

$$|\psi\rangle = \sum_{\{\alpha,m\}} \left[\cdots B_{\alpha_3\alpha_2}^{m_2} B_{\alpha_2\alpha_1}^{m_1} \cdots\right] |\cdots, m_2, m_1, \cdots\rangle. \quad (2)$$

The indices $0 \leq \alpha_i < \chi$ to be traced over are called 'auxiliary' indices, which we consider to be states in an 'auxiliary Hilbert space' defined on the bonds between sites. With the proper normalization, the auxiliary states are in one to one correspondence with the entanglement spectrum of a cut on the bond. An important insight from the classification scheme is that a suitable renormalization procedure[16,18] can be defined which produces a representative state of the smallest possible χ. For example, the $\chi = 2$ state of Affleck, Lieb, Kennedy and Tasaki (AKLT)[19] is representative of the SPT ordered Haldane phase[20] of the spin-1 Heisenberg chain.

The observed simplicity of the FQH model states' entanglement spectrum suggests they play an analogous role for the FQH effects as the AKLT state does for the Haldane phase. To pursue the analogy further, the 1+1D AKLT wave function can be written as a time ordered correlation function of a single '0 + 1D' spin-$\frac{1}{2}$, which leads to its simple expression as an MPS whose $\chi = 2$ auxiliary Hilbert space is a spin-$\frac{1}{2}$.[21] The 2+1D FQH model wave functions can be written as the correlation function of a 1+1D CFT. Does it follow that the model FQH states have exact representations as an MPS with an auxiliary Hilbert space in one to one correspondence with the CFT, and if so, can they be implemented and manipulated numerically?

In this paper we show that the model FQH wave functions and their quasiparticle excitations indeed have exact representations as MPSs. As expected the requisite

structure of the model states is that their wave functions are the correlation functions of a 1+1D CFT, which implies essentially by definition that they are MPSs whose auxiliary Hilbert space is the CFT. We also explain how the edge excitations and ground state degeneracy arise in the MPS picture.

Working on a cylinder in the Landau gauge, we can view the system as a 1D chain of orbitals for which the B-matrices of Eq. (2) are the matrix elements of local operators of the CFT. We have implemented these MPSs numerically for both the fermionic Laughlin and Moore-Read states on the geometry of an *infinitely* long cylinder of circumference L, allowing us to measure arbitrary real-space correlation functions using the standard infinite MPS algorithms. The infinite cylinder has a number numerical advantages, including the absence of boundaries, full translation invariance and no curvature effects. Compared to the torus geometry,[22–24] only a single cut is required to study the entanglement, greatly simplifying the identification of the entanglement spectrum. As we show in Sec. III, the computational complexity of the MPS representation is on the order $\mathcal{O}(b^L)$ for $b \sim \mathcal{O}(1)$. However, to achieve the same type of scaling in the traditional Hilbert space representation (say on a sphere[5,25–29]) would require $N \sim \mathcal{O}(L^2)$ particles and a Hilbert space dimension scaling as b^{L^2}. We also note that previously a conceptually distinct approach found an MPS for the Laughlin state in which there is one matrix per *particle*, rather than per orbital.[30] However, the construction does not generalize to other FQH states and again results in a complexity b^N, which implies it cannot be implemented on the infinite cylinder geometry.

In addition, we introduce an algorithm for calculating the real-space entanglement spectrum of any state given as an MPS in the orbital basis. We first use the larger system sizes provided by the MPS representation to extract the topological entanglement entropy (TEE) γ using four different methods; first using the conventional scaling of the entanglement entropy,[2,3]

$$S = \sum_a E_a e^{-E_a} = a_S L - \gamma + \mathcal{O}(L^{-1}), \qquad (3)$$

and second from a similar scaling form we derive for the lowest entanglement energy, $E_0 = a_E L - \gamma + \mathcal{O}(L^{-1})$, for both the orbital and real-space cuts. We find using E_0 in the orbital cut converges most quickly, and as this form is applicable to other topologically ordered phases, it may prove useful in cases where small system sizes are a constraint. We are able to definitively determine γ using all four methods for the $q = 3, 5$ and 7 Laughlin states, as well as the $q = 2$ Moore-Read state (*cf.* Tab. I), which proved difficult in previous studies.[23,25,26,28]

Finally, we perform a detailed scaling analysis of the spectrum for both the orbital and real-space cuts. During the final preparation of this work, a recent preprint[31] has conclusively demonstrated earlier arguments that the real-space entanglement spectrum of the model wave functions takes the form of the chiral Hamiltonian H per-
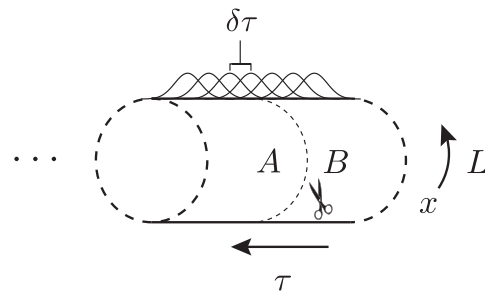

FIG. 1. The infinite cylinder geometry for model FQH wave functions. L is the circumference, x and τ are the coordinates around and along the cylinder respectively. $\delta\tau = \frac{2\pi\ell_B^2}{L}$ is the spacing between Landau level orbitals. A real-space entanglement cut between regions A, B would be made along some fixed τ.

	Filling	v_ϕ	v_χ	$\mathcal{D}^2 = e^{2\gamma}$
	1	2.2568 ± 0.0003		$|\gamma| < 10^{-7}$
Laughlin	1/3	1.2956 ± 0.0006		2.996
	1/5	0.672 ± 0.009		4.96
	1/7	0.28 ± 0.02		6.88
Moore-Read	1/2	1.33 ± 0.01	0.21 ± 0.01	7.77

TABLE I. Extracted real-space entanglement velocities and TEE γ for various model wave functions. v_ϕ is the velocity of the chiral boson, and for the MR case, v_χ the velocity of the chiral Majorana, in units of the magnetic length $\ell_B = (\hbar/qB)^{1/2}$. For the $\nu = 1$ integer quantum Hall state, the exact value of the velocity is known to be $4/\sqrt{\pi}$. In the column for total quantum dimension $\mathcal{D}$, we present the value extracted via the orbital cut E_0 around $L = 25\ell_B$. (For $\nu = 1$ integer case, we use the real-space cut S instead.) Refer to Sec. VI for details on our numerical methods.

turbed by local, irrelevant boundary operators.[6,29] This implies a scaling collapse of the entanglement spectrum in the limit $L \to \infty$ for fixed CFT level n. The large system sizes available here give the first detailed demonstration of this principle, allowing us to extract the entanglement velocities for both the Majorana and $U(1)$ modes of the MR state, as well as the form of the leading irrelevant corrections.

In contrast, in the orbital cut each entanglement eigenvalue scales as $E_a - E_0 \sim L^{-\zeta_a}$ which precludes the possibility of collapsing the spectrum. This is contrary to earlier indications that the orbital spectrum showed the same linear dispersion,[27] though the case studied there was the 'conformal limit' of bosonic wave functions on a finite sphere. Taking the analogous conformal limit of the cylinder is trivial, so our results apply to the conformal limit of fermionic wave functions on an infinite cylinder. Whether this is a difference between the bosonic and fermionic cases or due to the smaller system sizes of the earlier analysis is left open.

II. MODEL WAVEFUNCTIONS AND MATRIX PRODUCT STATES

A number of gapped model wave functions, including those of the FQH, can be written as the correlation functions of a field theory in one lower dimension.[32] In the 2+1D FQH effect, for example, the model wave functions are correlation functions of a 1+1D chiral conformal field theory (CFT).[8] Other examples with this structure include the AKLT states, the Toric code,[33] and certain BCS superconductors.[34] As we will illustrate in the case of the FQH effect, this structure implies that the state has an exact implementation as an MPS or a tensor network. The auxiliary Hilbert space of the tensor network is in correspondence with the Hilbert space of the associated lower dimensional field theory. In turn, the edge excitations and the entanglement spectrum of tensor networks are known to be closely related;[35] this relationship takes a particularly elegant form for the FQH effect due to the stringent constraints of conformal invariance in 2D.[31]

The simplest example is the Laughlin state on an infinite cylinder, which can be written as the correlation function of a chiral boson $\phi(z)$,[8]

$$\Psi_L(z_i) = \prod_{i<j}^N \sinh\left((z_i - z_j)\frac{\pi}{L}\right)^q e^{-\frac{1}{2\ell_B^2}\sum_i \tau_i^2} \tag{4}$$

$$= \left\langle \exp\left[i\sqrt{q}\sum_{a=1}^N \phi(z_a) - i\sqrt{q}\rho\int d^2z\,\phi(z)\right]\right\rangle_\phi.$$

Throughout we will use $z = x + i\tau$ as a complex coordinate on the cylinder, where x runs around its circumference of length L and τ runs along its length, as illustrated in Fig. 1. The filling fraction is $\nu = \frac{1}{q}$, the magnetic length is $\ell_B^2 = \frac{\hbar}{eB}$, and the density of electrons is $\rho = \frac{1}{2\pi\ell_B^2 q}$.

The chiral boson ϕ is a free field characterized by its correlation function on the plane or cylinder,

$$\langle\phi(z)\phi(z')\rangle_{\text{plane}} = -\log(z - z'),$$
$$\langle\phi(z)\phi(z')\rangle_{\text{cyl}} = -\log\sinh\left[\frac{\pi}{L}(z - z')\right]. \tag{5}$$

In addition to an insertion $e^{i\sqrt{q}\phi(z_i)}$ for each electron, it is necessary to include a neutralizing 'background charge' $\mathcal{O}_{bc} = -i\sqrt{q}\rho\int d^2z\,\phi(z)$. The background charge introduces some subtleties, as the branch cut in the bosonic propagator has a phase ambiguity equivalent to a choice of gauge for the electrons, which we will address at a later point.

We can write a second quantized version of Eq. (4) using a coherent state wave function in the variable ψ (which is a complex/Grassmann number for bosons/fermions), which in the thermodynamic limit is

$$\Psi_L[\psi] = \langle 0|e^{\int d^2z\,\psi(z)\hat\Psi(z)}|\Psi_L\rangle$$
$$= \left\langle e^{\int d^2z[e^{i\sqrt{q}\phi(z)}\psi(z) - i\sqrt{q}\rho\phi(z)]}\right\rangle_\phi. \tag{6}$$

The notation is rather subtle as we are tying together two theories: the physical particles in 2+1D, with coherent state coordinate $\psi(z)$, and the path integral over the auxiliary space of the 1+1D chiral boson ϕ, characterized by the correlation functions $\langle\cdot\rangle_\phi$. Number conservation is enforced by the $U(1)$ symmetry of the chiral boson.

The structure of Eq. (6) is identical to that of a 'continuous matrix product state' (cMPS) defined in Ref. 36, which we review briefly. Starting with a lattice system of bosons or fermions at sites with positions τ, we first pass from the occupation basis $\{|m_\tau\rangle\}$ to the coherent state basis $\{|\psi_\tau\rangle\}$ by defining

$$B_{\alpha\alpha'}[\psi_\tau] \equiv \sum_{m_\tau}\langle\psi_\tau|B_{\alpha\alpha'}^{m_\tau}|m_\tau\rangle. \tag{7}$$

Second, we note that the trace over the auxiliary states $\{\alpha\}$ is formally equivalent to a path integral over a 1D system, with the B playing the role of transfer matrices. Anticipating the continuum limit, we assume there are matrices H, V in the auxiliary Hilbert space such that $B[\psi(\tau)] = e^{H(\tau)+V(\tau)\psi(\tau)}$. We can then take the continuum limit of the MPS by analogy to the usual time-ordered path integral, which defines a cMPS,

$$\Psi[\psi] = \text{Tr}_{\text{aux}}\left[\mathcal{T}e^{\int_0^{L_\tau}d\tau[H(\tau)+V(\tau)\psi(\tau)]}\right]. \tag{8}$$

Comparing the cMPS to the second quantized version of the Laughlin state, (6), we see that they are equivalent if we take the *physical* Hilbert space at each slice to be that of particles on a ring of circumference L, and the auxiliary Hilbert space to be that of a chiral boson. In this case, H is precisely the Hamiltonian of the chiral boson (plus the background charge $\mathcal{O}_{bc}$), while V is a vertex operator, $e^{i\sqrt{q}\phi}$. This structure was also recently noted in Ref. 31, where, in the MPS language, they find the dominant eigenvector of the 'transfer matrix'[13] of the cMPS, from which the entanglement Hamiltonian follows.

While the cMPS representation is convenient from an analytic perspective, computationally it is desirable to have the discrete version expressed in the basis of lowest Landau level (LLL) orbitals. Letting $w = e^{-\frac{2\pi i}{L}z}$, in Landau gauge the orbitals can be written as

$$\varphi_n(z) \propto e^{-\frac{1}{\ell_B^2}\left(i\tau_n x + \frac{1}{2}(\tau-\tau_n)^2\right)} = w^n e^{-\frac{1}{2\ell_B^2}(\tau_n^2+\tau^2)}, \tag{9}$$

where $\tau_n = \frac{2\pi n}{L}\ell_B^2$ is the guiding center for the nth orbital. Viewing the orbitals as the sites of an infinite 1D chain, we want to arrive at a discrete MPS as defined in (2), which requires finding the appropriate matrices $B_{\alpha\alpha'}^m$. Based on the cMPS, we expect α will be in one-to-one correspondence with the states of the associated CFT.

In order to extract the occupation number at orbital n, we take advantage of the fact that orbitals of the LLL (in the Landau gauge) are labeled by momentum. When acting on a many-body state in the LLL, we can then

replace the destruction operator $\hat{\psi}_n$ for orbital n with a contour integral around the cylinder,

$$\hat{\psi}_n \longrightarrow e^{\frac{\tau_n^2}{\ell_B^2}} \oint_{\tau=\tau_n} \frac{dw}{2\pi i} \, w^{-n-1} \hat{\psi}(w). \tag{10}$$

We chose to perform the integrals at τ_n, though with an appropriate change in normalization a different location could be chosen.

The gauge of the cMPS, however, depends on a branch cut prescription for the background charge. It is convenient to choose the cut to consistently occur at some fixed x coordinate, such as the boundary of $-L/2 < x < L/2$. This choice of gauge does not produce the Landau gauge; they differ by a phase $e^{ix\tau\ell_B^{-2}}$. Choosing this branch cut prescription for $\phi(z)$, but keeping ψ_n to be the destruction operators for the Landau gauge, we find the Laughlin and Moore-Read states can be brought to the form

$$\Psi[\psi_n] = \left\langle e^{\sum_n \oint_{\tau=\tau_n} \frac{dw}{2\pi i} \, w^{-1} \left[\mathcal{V}(w)\psi_n - \frac{i}{\sqrt{q}}\phi(w) \right]} \right\rangle_{\text{CFT}}, \tag{11}$$

where

$$\mathcal{V}(w) = e^{i\sqrt{q}\phi(w)} \quad \text{(Laughlin)}, \tag{12a}$$

$$\mathcal{V}(w) = \chi(w)e^{i\sqrt{q}\phi(w)} \quad \text{(Moore-Read)}. \tag{12b}$$

Eq. (11) looks like free time evolution governed by the Hamiltonian of the chiral CFT, H, punctuated by interactions at τ_n. As orbital ordering coincides with time ordering, we can pass to the Hamiltonian picture by inserting resolutions of the identity $\mathbb{1} = \sum_\alpha |\alpha\rangle\langle\alpha|$ at positions $\tau = \tau_n \pm \epsilon$, where α label all states of the CFT. A resulting unit cell looks like

$$\Psi[\psi_n] = \sum_{\{\alpha\}} \Bigg[\cdots \langle\alpha_{n+1}|e^{-\delta\tau H}|\alpha_n\rangle$$
$$\langle\alpha_n|e^{\mathcal{V}_0\psi_n - \frac{i}{\sqrt{q}}\phi_0}|\alpha_{n-1}\rangle \cdots \Bigg], \tag{13}$$

where the operator

$$\hat{\mathcal{V}}_0 \equiv \oint \frac{dw}{2\pi i} \, w^{-1} \mathcal{V}(w) \tag{14}$$

is precisely the '0$^{\text{th}}$ mode' of the operator $\mathcal{V}(w)$, and likewise ϕ_0 is the zero-mode of the chiral boson.

The resulting transfer operators are of two types. For the 'free' segments $\tau \in (\tau_n, \tau_{n-1})$, the transfer operator is

$$U(\delta\tau) \equiv e^{-\delta\tau H}, \quad U(\delta\tau)_{\alpha\beta} = \delta_{\alpha\beta} e^{-\delta\tau E_\alpha} \tag{15}$$

where α again runs over states of the CFT, with energies E_α, and $\delta\tau = \frac{2\pi}{L}\ell_B^2$. At the location of each site we define a transfer operator

$$T_{\alpha\alpha'}[\psi_n] \equiv \langle\alpha|e^{\hat{\mathcal{V}}_0\psi_n - \frac{i}{\sqrt{q}}\phi_0}|\alpha'\rangle \tag{16}$$

(a)Structure of the orbital MPS.

(b)Definition of the B-matrix.
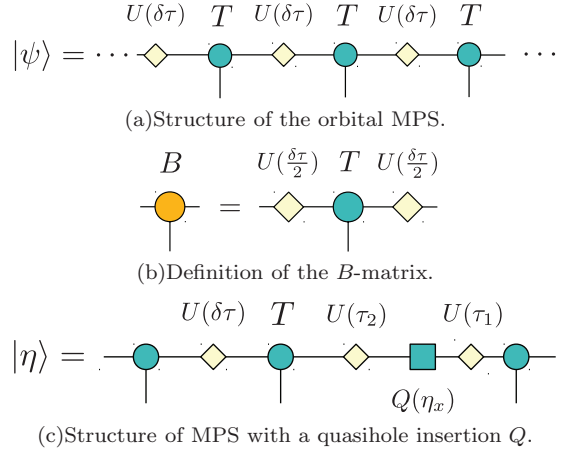

(c)Structure of MPS with a quasihole insertion Q.

FIG. 2. The structure of the orbital MPS. (a) U is free time evolution of the CFT, punctuated by perturbations T at $\tau = \tau_n$. (b) The B-matrices are defined by combining U and T. (c) A quasiparticle is inserted by placing the matrix elements of the vertex operator Q in the correct time-ordered positions. It can be absorbed into either of the adjoining B-matrices.

Stringing the transfer matrices together, we arrive at the exact MPS,

$$\Psi[\psi_n] = \prod_n U(\delta\tau) T[\psi_n]. \tag{17}$$

as illustrated in Fig. 2(a). We have suppressed the implicit summation over the CFT states α. The above is in 'coherent state' form; to convert to the occupation basis, $\{|m\rangle\}$ we define the usual occupation basis B-matrices as

$$\sum_m B^m (m!)^{\frac{3}{2}} \psi^m \equiv U(\tfrac{1}{2}\delta\tau) \, T[\psi] \, U(\tfrac{1}{2}\delta\tau) \tag{18}$$

as shown in Fig. 2(b). Because the Laughlin and Moore-Read states are described by free CFTs, both T and U, and hence B, can be calculated exactly at negligible numerical cost (for the details of this calculation, we refer to Appendices A and B). For an arbitrary CFT, their calculation is more involved but nevertheless tractable using formulas developed for the 'truncated conformal space' approach to perturbed CFTs.[37]

In order to obtain wave functions on a half or finite cylinder, one simply truncates the MPS using the vacuum of the CFT as a boundary condition for the severed auxiliary bonds. If neutral excited states are used as the boundary condition, these produce the corresponding model edge excitations.[38] This structure is analogous to the spin-$\frac{1}{2}$ degree of freedom at the boundary of an AKLT chain, which arises from the two choices of boundary condition for the $\chi = 2$ MPS.

The ground state degeneracy of the phase can also be understood. If the phase is d-fold degenerate, it is known[39] that there are d-primary fields in the CFT, and the states of the CFT partition into d families which 'descend' from each of these primary fields. Each family is

invariant under the action of the electron operator $\mathcal{V}(w)$, so it follows that a given bond can be consistently truncated to one of these d families. The d choices on the bond provide the d 'minimal entanglement states'.[40] Appendices A and B include a more detailed explanation.

The 'thin torus' wave functions can also be understood as a limiting case of our construction.[41,42] If we truncate the MPS by keeping only the 'highest weight' states of the CFT, i.e., those of the lowest energy within each family of the CFT, we arrive at a $\chi = 1$ MPS. We also note that an approximate $\chi = 2$ MPS for the Laughlin state was recently found;[43] in our language this can be understood as truncating the CFT to the states $|P| \leq 1$.

We now explain how the two conserved quantities of the LLL problem, particle number and momentum (sometimes called 'center of mass'), can be assigned to the states of the CFT. In the orbital basis we define the conserved quantities to be

$$\hat{C} = \sum_j q\hat{N}_j - p \quad \text{(particle number)}, \tag{19a}$$

$$\hat{K} = \sum_j j(q\hat{N}_j - p) \quad \text{(momentum)}, \tag{19b}$$

where j is the orbital index and we have included a filling factor dependent scaling ($\nu = p/q$) so that both remain finite in the thermodynamic limit. If a state is invariant under a $U(1)$ symmetry transformation, the states of the Schmidt spectrum can be assigned definite charge. Consequently, the entanglement spectrum on bond $\bar{n} \in \mathbb{Z} + \frac{1}{2}$ can be labeled by pairs $(C_{\bar{n}}, K_{\bar{n}})$. The states of the auxiliary CFT have quantum numbers as well, in particular the total momentum $|P|$ of the CFT and the winding number N of the boson (see Appendix A for detailed definitions). The pairs $(N, |P|)$ and $(C_{\bar{n}}, K_{\bar{n}})$ are related by

$$C_{\bar{n}} = N, \tag{20a}$$

$$K_{\bar{n}} = q|P| + \frac{1}{2}N^2 + \bar{n}N, \tag{20b}$$

which explains how the previously observed offsets of the $|P| = 0$ levels depend on the number sector and bond location.

III. CONVERGENCE PROPERTIES AND COMPUTATIONAL COMPLEXITY

For numerical purposes we must truncate the MPS by keeping only the χ most important states in the entanglement spectrum. Most MPS algorithms (such as measuring correlation functions) can then be computed with time $\mathcal{O}(M\chi^3)$ and storage $\mathcal{O}(\chi^2)$, where M is the number of sites involved in the measurement. We argue that to simulate the state at some fixed precision we must keep $\chi \sim e^{\alpha cL/v}(cL/v)^{-1/2}$ where c is the central charge of the entanglement spectrum, v is its 'entanglement velocity,'
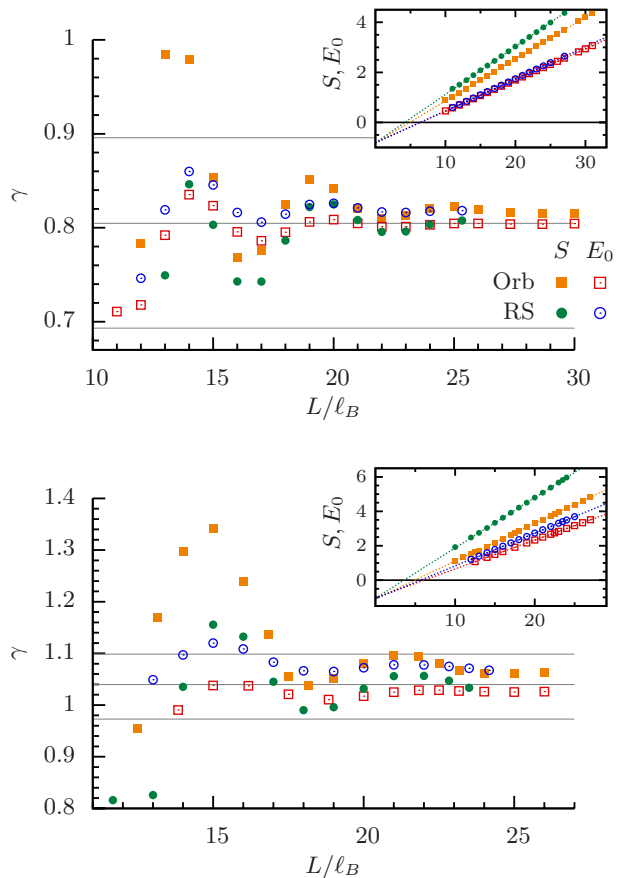

FIG. 3. Numerically computing the TEE γ for the $\nu = 1/5$ Laughlin state (top) and the $\nu = 1/2$ Moore-Read state (bottom). γ is extracted from both orbital (squares) and real-space (circles) cut, via the entanglement entropy S (filled) and the lowest entanglement energy E_0 (empty), by performing windowed fits to the form $S(L), E_0(L) = a_{S,E}L - \gamma$ at various circumferences L. The horizontal lines marks the values of $\gamma = \log \mathcal{D}$ where $\mathcal{D}^2 = 4, 5, 6$ (top) and $7, 8, 9$ (bottom). As $L \to \infty$, the extracted value of γ approaches their theoretical values of $\frac{1}{2}\log 5$ and $\frac{1}{2}\log 8$ respectively. In the latter case we can see that $L \gtrsim 20\ell_B$ is required for the TEE to be extracted with reasonable accuracy. (Insets) S vs. L/ℓ_B for the four cases.

and α is a non-universal constant of order 1. In contrast to exact diagonalization, the complexity scales exponentially only in the circumference of the cylinder, rather than its area. Use of the conserved quantum numbers drastically reduces the computational time, but does not alter the exponential complexity.

Following Kitaev and Preskill's derivation of the topological entanglement entropy,[2] we proceed under the assumption that the 'thermodynamic' properties of the entanglement spectrum, such as the entanglement entropy, take the same form as those of the auxiliary CFT. However, there is no reason to expect the velocities that appear will be universal, so in what follows all powers of L/v should be understood to have non-universal coefficients.

The exact status of this assumption for the orbital basis is somewhat unclear, because as we will show the orbital spectrum does not collapse to the CFT; nevertheless the appearance of γ in the entropy S, the scaling form of the lowest eigenvalue E_0, and the collapse we find for the convergence of S with increased χ appear to behave as expected.

The density of states $\rho(E)$ for a modularly invariant CFT is given by the 'Cardy' formula.[44] However, we must take into account the fact that only the identity sector of the CFT, '$\mathbb{1}$', belongs to the entanglement spectrum (at least for the 'minimally entangled'[40] ground states). The corresponding partition function and density operator are defined as

$$\mathcal{Z}_1 = \mathrm{Tr}_{\mathbb{1}}\, e^{-\beta H_e}, \tag{21}$$

$$\hat{\rho} = \mathcal{Z}_1^{-1}\, \mathrm{Tr}_{\mathbb{1}}\, e^{-H_e}. \tag{22}$$

The derivation of the Cardy formula requires a modular transformation, but the required partition function is not modularly invariant. This results in the explicit appearance of the modular $\mathcal{S}$ matrix, $-\log(S_1^1) = \gamma$, where γ is the topological entanglement entropy. Taking this term into account, the density of states is

$$\rho(E)dE = \frac{dE}{4E}\sqrt{\frac{2}{\pi}}e^{-\gamma}e^{\sqrt{\frac{\pi(c+\bar{c})EL}{3v}}}\left(\frac{\pi(c+\bar{c})EL}{3v}\right)^{1/4}. \tag{23}$$

All the other thermodynamic properties follow from $\rho(E)$. It is convenient to introduce the dimensionless variable μ,

$$\mu \equiv \left(\frac{\pi(c+\bar{c})EL}{3v}\right)^{1/4}. \tag{24}$$

We can calculate the partition function and entanglement entropy,

$$\mathcal{Z}(\beta) = \int \rho(E)e^{-\beta E}dE$$
$$= \sqrt{\frac{2}{\pi}}e^{-\gamma}\int e^{\mu^2 - \frac{3v}{\pi(c+\bar{c})}\frac{\beta}{L}\mu^4}d\mu$$
$$= e^{\frac{\pi(c+\bar{c})}{12}\frac{L}{\beta v}-\gamma+\cdots}, \tag{25}$$
$$S = \partial_{\beta^{-1}}(-\beta^{-1}\ln \mathcal{Z})\big|_{\beta=1}$$
$$= \frac{\pi(c+\bar{c})}{6}\frac{L}{v}-\gamma+\cdots. \tag{26}$$

The partition function (25) is evaluated via steepest descent about the saddle point $\mu_* = \sqrt{\frac{\pi(c+\bar{c})}{6v}\frac{L}{\beta}}$. As the entanglement spectrum is $p_i = e^{-E_i}/\mathcal{Z}(1)$, a particular consequence of Eq. (25) is that the lowest entanglement level is $p_0 = e^{-[a_E L-\gamma]}$ for some non-universal a_E. A similar result was recently obtained in.[31] As illustrated in Fig. 3, for both the orbital and real-space cuts γ can be extracted from the scaling of p_0 with equivalent or better accuracy as from S.
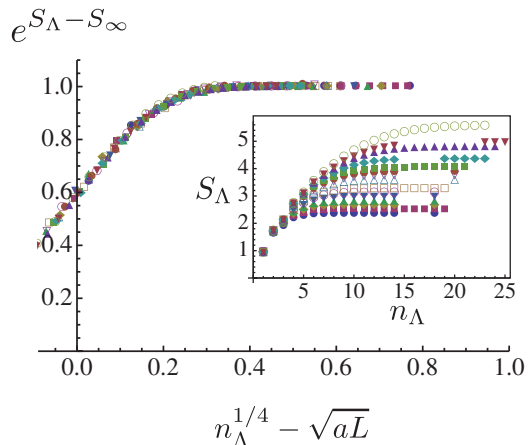
$$e^{S_\Lambda - S_\infty}$$

$$n_\Lambda^{1/4} - \sqrt{aL}$$

FIG. 4. Convergence of the orbital entanglement entropy S_Λ for the $q=3$ Laughlin state as the number of Virasoro levels kept (n_Λ) is increased. (Inset) For various circumferences $19\ell_B \leq L \leq 40\ell_B$, we calculate the entanglement S_Λ of the MPS keeping only the lowest n_Λ Virasoro levels of the CFT. For large enough n_Λ, S_Λ converges to the exact entanglement entropy S_∞. We expect the convergence to be controlled by the parameter $\mu - \mu_* \propto n_\Lambda^{1/4} - (aL)^{1/2}$ for some a. (Main figure) We plot the convergence of the entanglement entropy, $e^{S_\Lambda - S_\infty}$ as a function of $n_\Lambda^{1/4}-(aL)^{1/2}$, with $a \approx 0.0875$ giving a good collapse.

The steepest descent analysis shows that the bulk of the probability comes from a region within $\mathcal{O}(1)$ of the saddle point μ_*. At this point the number of states χ with $E < E_*$ is

$$\chi(E_*) = \int^{E_*}\rho(E)\,dE \sim \frac{e^{-\gamma}}{\sqrt{2\pi}}\frac{e^{\frac{\pi(c+\bar{c})}{6}\frac{L}{v}}}{\sqrt{\frac{\pi(c+\bar{c})}{6}\frac{L}{v}}}. \tag{27}$$

Alternately, we can define the number of CFT Virasoro levels n_* required above the vacuum state,

$$n_* \equiv \frac{E_* L}{2\pi v} = \frac{(c+\bar{c})}{24}\left(\frac{L}{v}\right)^2. \tag{28}$$

To study the convergence properties, suppose we only keep states such that $E < E_\Lambda$. The cutoff partition function $\mathcal{Z}_\Lambda$ is

$$\mathcal{Z}_\Lambda(\beta) = \int^{E_\Lambda}dE\,\rho(E)\,e^{-\beta E}$$
$$\sim \mathcal{Z}_\infty(\beta)\frac{1}{2}\mathrm{erfc}\left(-\sqrt{2}(\mu_\Lambda - \mu_*)\right), \tag{29}$$

with resulting truncation error

$$\epsilon_\Lambda \equiv 1 - \frac{\mathcal{Z}_\Lambda(1)}{\mathcal{Z}_\infty(1)} = \frac{1}{2}\mathrm{erfc}\left(\sqrt{2}(\mu_\Lambda - \mu_*)\right). \tag{30}$$

While the specific functional form may not remain universal, it suggests that convergence is controlled by the dimensionless factor $\mu_\Lambda - \mu_* \sim n_\Lambda^{1/4} - (aL)^{1/2}$. In the

inset of Fig. 4, we plot the convergence of the entanglement entropy S_Λ as a function of the number of Virasoro levels n_Λ kept at various circumferences L. We then scale the data horizontally by plotting as a function of $n_\Lambda^{1/4} - (aL)^{1/2}$ for a numerically fit value of a. Without any further *vertical* scaling, the data appears to collapse. This is somewhat surprising given the irregular structure of the orbital spectrum, but does validate the predicted form $n_\Lambda \sim L^2$. Choosing an acceptable fractional error for S_Λ, in large L limit we then conclude from the Cardy formula the required dimension of the MPS to simulate at fixed accuracy is

$$\chi \sim e^{\alpha cL/v}(cL/v)^{-1/2} \qquad (31)$$

as claimed.

IV. QUASI-PARTICLE EXCITATIONS

We now discuss how to introduce quasiparticles into the MPS. In the 'conformal block' approach to model wave functions,[8] a quasiparticle excitation at η is introduced by inserting an appropriate operator $\mathcal{Q}(\eta)$ into the CFT correlator,

$$\Psi[\psi_n; \eta] = \left\langle \mathcal{Q}(\eta) e^{\sum_n \left[\mathcal{V}_0(\tau_n)\psi_n - \frac{i}{\sqrt{q}}\phi_0(\tau_n)\right]} \right\rangle_{\text{CFT}}. \qquad (32)$$

We will focus on the Laughlin and Moore-Read quasiholes, for which $\mathcal{Q}$ is a *local* operator that takes a particularly simple form,

$$\mathcal{Q}(\eta) = e^{i\phi(\eta)/\sqrt{q}} \quad \text{(Laughlin)}, \qquad (33a)$$

$$\mathcal{Q}(\eta) = \sigma(\eta)e^{i\phi(\eta)/2\sqrt{q}} \quad \text{(Moore-Read)}. \qquad (33b)$$

Here $\sigma(\eta)$ is the chiral part of the Ising order operator. Quasiparticles require 'quasi-local' operators,[45] which can also be included in the MPS, but we have deferred their implementation.

To incorporate the quasihole into the MPS, we first explicitly time order Eq. (32) by bringing the insertion $\mathcal{Q}(\eta)$ between the orbitals $\tau_{n+1} \geq \eta_\tau \geq \tau_n$. For fermions, this introduces a sign for each electron in the region $\tau > \eta_\tau$. As detailed in Appendix D, this sign can be written as $s^{\hat{\pi}_0/\sqrt{q}}$, where $\hat{\pi}_0$ is conjugate to the bosonic zero-mode and $s = \pm 1$ for bosons and fermions respectively.

We calculate the matrix elements of $\mathcal{Q}$ at $\tau = 0$,

$$Q_{\alpha,\beta} = \langle \alpha | s^{\hat{\pi}_0/\sqrt{q}} \mathcal{Q}(\eta_x) | \beta \rangle, \qquad (34)$$

and then insert Q into the 'free' evolution on the bond between sites $n, n+1$,

$$U(\delta\tau) \rightarrow U(\tau_a) Q U(\tau_b), \ \ \tau_a + \tau_b = \delta\tau, \qquad (35)$$

where $\tau_a = \tau_{n+1} - \eta_\tau$. The structure of the resulting MPS is illustrated in Fig. 2(c). For further details on calculating Q for the Laughlin and MR states we refer to Appendix D.
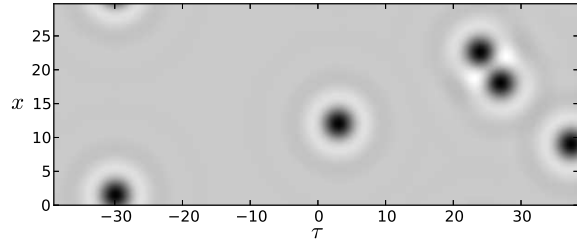

FIG. 5. The real-space density $\rho(\tau, x)$ of a $q = 5$ Laughlin state with five quasi-holes on an infinite cylinder of circumference $L = 30\ell_B$. Distances are measured in units of ℓ_B. (The top and bottom edges are identified.)

We have implemented the Laughlin quasiholes numerically, with a resulting density profile for a collection of quasiholes in the $q = 5$ state shown in Fig. 5. As a simple test of the result, we can explicitly evaluate the Berry connection associated with the transport of one quasihole around another,

$$\theta = \oint dA = \oint d\eta \langle \eta | (-i\partial_\eta) | \eta \rangle. \qquad (36)$$

We keep one quasihole fixed at $\eta = 0$, while a second follows a discretized path η_i chosen to wind around the other, which defines a discretized connection $e^{iA_{ij}} = \langle \eta_i | \eta_j \rangle$. We then integrate the connection after subtracting out a similar phase in the absence of the second particle. Calculating the inner product between two matrix product states can be computed with complexity $\mathcal{O}(A/\ell_B^2 \, \chi^3)$, where A is the area of the region enclosing the quasiholes in question. Working on an $L = 16\ell_B$ cylinder and ensuring the quasiparticles remain at least a distance of $8\ell_B$ apart, we find a statistical angle $\theta_{q=3} = 2.0992$, compared to the prediction of $\frac{2\pi}{3} = 2.0944$. The computation takes about 1 minute.

While the result is already well established for the Laughlin states,[46] it would be worthwhile to explicitly calculate the non-abelian Berry connection for the Moore-Read quasiparticles. As we have computed the form of the Q-matrices, we believe this would be tractable.

V. REAL-SPACE ENTANGLEMENT SPECTRUM

Finally, we present an algorithm for computing the real-space entanglement spectrum (RSES) of quantum Hall states on both finite and infinite cylinders. In contrast to the orbital cut,[25] which cuts the system into two sets of LLL orbitals, in the real-space cut we cut the system into two regions of physical space. Previously this was accomplished analytically for the free $\nu = 1$ case,[47,48], numerically using Monte Carlo[49], and large scale SVD of explicit wave functions.[28,29] Our technique
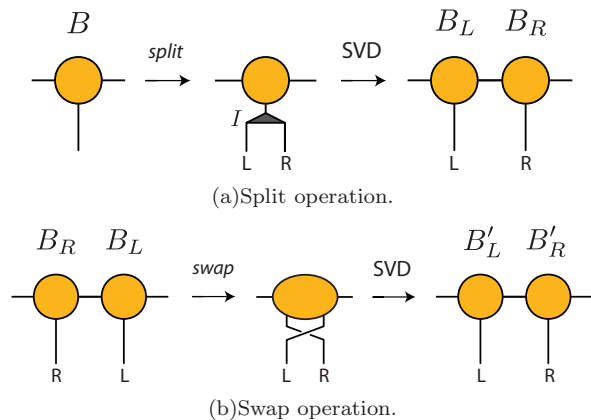
(a)Split operation.

(b)Swap operation.

FIG. 6. The splitting and swapping procedure performed on an MPS. The two operations allow us to compute the real-space entanglement cut from an orbital MPS.

is not specific to the model wave functions, and provides a means for computing the RSES of non-model states calculated from DMRG. As the scaling form of the entanglement spectrum only appears for the real-space cut, this may prove an important diagnostic for non-model states. For simplicity, we assume a wave function in the LLL, and consider an entanglement cut running around the cylinder at $\tau = \tau_c$.

The first step of the algorithm is to 'split' each orbital $\varphi_n(z)$ [Eq. (9)] into components $\varphi_{nR/L}$ supported on the right and left of a cut at τ_c,

$$\varphi_n(z) = \theta(\tau - \tau_c)\varphi_n(z) + \theta(\tau_c - \tau)\varphi_n(z)$$
$$= g_{nL}\varphi_{nL}(z) + g_{nR}\varphi_{nR}(z). \quad (37)$$

We normalize the split orbitals by factors $g_{L/R}$ such that $\{\varphi_{nL}, \varphi_{nR}\}$ remains an orthonormal basis. Expressing the state in terms of the 'split' basis amount to appending isometries I onto the B-matrices,

$$B^m_{\alpha\beta} \to B^m_{\alpha\beta}I^{kl}_m, \quad I^{kl}_m = \sqrt{\binom{m}{k}} g^k_L g^l_R \, \delta_{k+l,m}, \quad (38)$$

where the factors g implicitly depend on the orbital location. Because the orbitals φ_n are exponentially localized about $\tau_n = \frac{2\pi\ell_B^2}{L}n$, we can work at some fixed accuracy by splitting only the $M \sim \mathcal{O}\left(\frac{L}{\ell_B}\right)$ orbitals nearest to the cut. In practice, we find $M = 1.5L/\ell_B$ is sufficient to obtain a converged spectrum. As illustrated in Fig. 6(a), the affected B matrices are then split using a singular value decomposition (SVD) equivalent to the truncation step of time evolving block decimation (TEBD).[50] As with TEBD, the splitting step preserves the 'canonical' form of the MPS, implying that the bipartition about the new bond is a Schmidt decomposition.

After the splitting step we have added M B-matrices to the chain, with orbitals alternating between the left and right sides of the cut. Choosing some particular bond to represent the location of the cut (usually the bond at the

center of the set of sites we have split), we sort the MPS through a series of $\mathcal{O}(M^2)$ swapping procedures, bringing all indices associated to the left region to the left of the cut, and likewise for the right. As illustrated in Fig. 6(b), for each swap we form a two-site wave function, permute the right and left legs to bring them to the desired order, and then split the wave function using SVD to obtain a new pair of B-matrices. Again, the canonical form of the MPS is preserved during this procedure, so after performing the required swaps the bond designated as the cut gives the real-space Schmidt decomposition.

Depending on the initial bond dimension χ, it may be necessary to truncate the new B-matrices by keeping only the largest singular values of the SVD. It appears that the low lying states are not affected by truncation of the highest lying states, but the convergence with increased χ should be checked on a case by case basis.

VI. ENTANGLEMENT SPECTRUM: ORBITAL CUT VS. REAL-SPACE CUT

In this section we study the scaling form of the RSES, then contrast it to the orbital spectrum. As illustrated for the $q = 3$ Laughlin state in Figs. 7, and for the MR state in Figs. 11, the orbital and real-space cuts agree in their counting, which is that of the CFT, but differ in the scaling of the energy levels E_i present in the spectrum.

Kitaev and Preskill[2] first noted that the known universal features of topological entanglement entropy could be explained if the *energies* of the entanglement spectrum coincided with those of the chiral CFT. A physical argument was later provided in Ref. 6. Recall that the states of the CFT are grouped into 'families' associated with each primary field ϕ_h,[39] in this context one per degenerate ground state on a cylinder, and let $\hat{P}_{\phi_h}$ denote a projection operator onto the corresponding family. The basic conclusion of Ref. 6 was that the reduced *real-space* density matrix of a topological state with gapless chiral edge modes takes the form

$$\hat{\rho}_L = \sum_h p_h \hat{P}_{\phi_h} e^{-v\hat{H}+\mathcal{O}(k\ell_B)} \hat{P}_{\phi_h}. \quad (39)$$

Here $\hat{H}$ is the Hamiltonian of the CFT, which we will take to have velocity 1, so an 'entanglement velocity' is included as a factor v. $\hat{H}$ is perturbed by more irrelevant boundary operators of order $(k\ell_B)^\nu$ for $\nu > 1$. The coefficients p_h depend on the degenerate ground state being considered. During the final preparation of this work, this scaling form was put on firm footing for the model FQH states.[31]

While the irrelevant operators generally introduce 'interaction terms' to the entanglement Hamiltonian, to illustrate the expected behavior we consider the simplest type of correction, a dispersive term. For the Laughlin
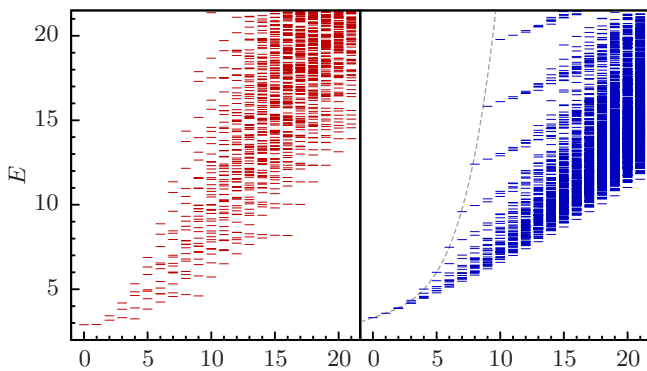
FIG. 7. Entanglement spectra (in the neutral charge sector) of the orbital (left) and real-space (right) cut of the $q = 3$ Laughlin state at $L = 32\ell_B$. The energies E are plot against their momentum in units of $\Delta k = \frac{2\pi}{L}$. Both spectra have the counting 1, 1, 2, 3, 5, 7, 11, *etc.*, consistent with that of a chiral boson CFT. However, the energy levels E have vastly different quantitative behaviors in the two cases, which we investigate in Fig. 8. The dashed line on the right is of the form $v\epsilon(k) = vk[1 + u_2 k^2 + u_4 k^4]$, with u_2, u_4 fit from the highest level of each sector, which we associate to the state $a_n^\dagger|0\rangle$. The fits appear to rule out a similar term u_1, but larger sizes and a treatment of the 'interactions' would be required to rule at u_3 if it is indeed absent.

state this takes the form

$$\tilde{E}_a \equiv E_a - E_0 \sim v\left[\sum_{n>0} \epsilon(k_n)a_n^\dagger a_n + \frac{2\pi}{L}\frac{\hat{N}^2}{2q}\right], \quad (40)$$

$$\epsilon(k) = k[1 + u_2 k^2 + u_4 k^4 + \cdots], \quad k_n = \frac{2\pi}{L}n. \quad (41)$$

which accounts for the 'branches' apparent in the real-space spectrum (Fig. 7 right), each of which is associated with the presence of a new mode $a_n^\dagger$. The dispersion relation can be fit from the heights of these branches. Note that only odd powers of k can appear in the dispersion of a chiral boson. In general, if the irrelevant perturbations descend from the identity boundary operator, only odd powers in k should appear.

In order to accurately extract the entanglement velocity, we consider the scaling of the shifted spectrum $\frac{\tilde{E}L}{2\pi}$ with increased L. Based on these scaling ideas, a state with momentum $k = \frac{2\pi}{L}(n_\phi + n_\chi)$ should have an energy

$$\frac{\tilde{E}_a L}{2\pi} = v_\phi(\Delta_{\phi h} + n_\phi) + v_\chi(\Delta_{\chi h} + n_\chi)$$
$$+ t_{2a}L^{-2} + t_{4a}L^{-4} + \cdots \quad (42)$$

where n_ϕ and n_χ are integers corresponding to the momenta of the $U(1)$ and Majorana sectors. The offsets $\Delta_{\phi/\chi h}$ are the scaling dimensions of the highest weight state in the sector, which depends on the bond and number sector in question (for the Laughlin states, it is $\frac{N^2}{2q}$). For the MR case we have included a detailed exposition of this structure in Appendix C.

(a)Real-space cut: plot of $\tilde{E}L/2\pi$ vs. $-1/L^2$.

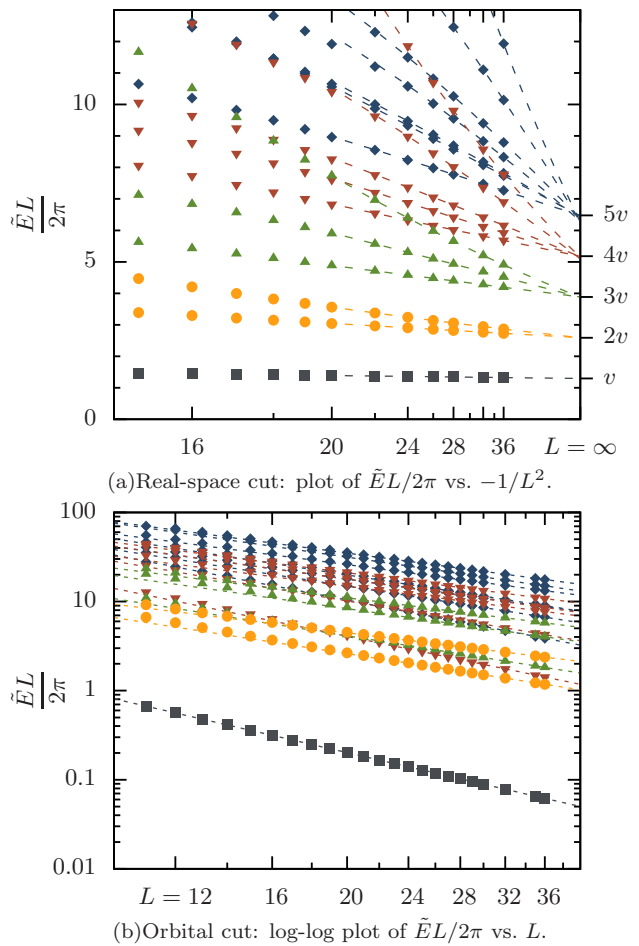(b)Orbital cut: log-log plot of $\tilde{E}L/2\pi$ vs. L.

FIG. 8. The relative entanglement energies for the real-space cut and orbital cut of the Laughlin state at $\nu = 1/3$. (Data shown for the charge neutral sector, L shown in units of ℓ_B.) The states at different momenta are distinguished by their colored symbols. (a) For the real-space cut, we plot $\frac{\tilde{E}L}{2\pi}$; the relative entanglement energy (relative to E_0) times the cylinder radius, as a function of $-1/L^2$. The energies are extrapolated to $L = \infty$ using a quadratic fit $t_0 + t_2 L^{-2} + t_4 L^{-4}$, and land on multiples of the entanglement velocity $v \approx 1.2956$. (b) For the orbital cut, we show $\frac{\tilde{E}L}{2\pi}$ on a log-log plot, showing that the data has a linear behavior with negative slopes. The lines shown results from a linear fit to the last few data points. This demonstrates a nonlinear relation $\tilde{E}_a \propto L^{-\zeta_a}$ with $\zeta_a > 1$.

Focusing on the identity sector $\Delta_h = 0$ of the *real-space* $q = 3$ Laughlin cut, Fig. 8(a) tracks the scaled relative entanglement energy levels $\frac{\tilde{E}L}{2\pi}$ as a function of L^{-2}, extrapolating their value as the circumference approaches infinity. As indicated by the right-most tics of the figure, $\frac{\tilde{E}L}{2\pi}$ approaches $n_\phi v_\phi$ for large L, where $v_\phi \approx 1.2956$. The data clearly confirms that the real-space entanglement spectrum approaches a linear dispersion with fixed velocity, and the success of the fit justifies the absence of L^{-1} and L^{-3} perturbative terms. We have tabulated the velocities for the $q = 1, 3, 5$ and 7 in table I. The relation $v_{q=1}/v_{q=3} \approx \sqrt{3}$ noted previously[28] appears not
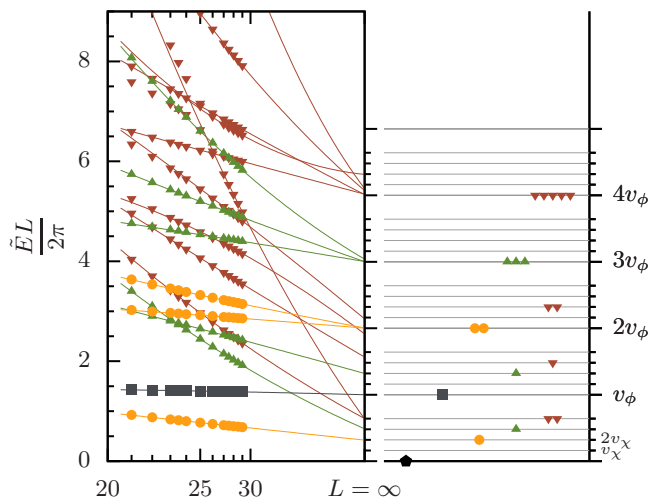
FIG. 9. Extrapolating the entanglement energies $\tilde{E}L/2\pi$ for the Moore-Read state at $\nu = 1/2$, using a cut associated with counting 1, 1, 3, 5, 10, *etc.* for $N = 0$ charge sector (*cf.* App. C). (Left) Here we show that the energies for the first three momenta extrapolate to integral combinations of v_ϕ and v_χ, the velocities of the chiral boson and Majorana mode respectively. The major tics on the vertical axis labels multiples of v_ϕ, the minor tics label combinations $n_\phi v_\phi + n_\chi v_\chi$ for integers n_ϕ and n_χ (and ℓ_B set to 1). States with momentum $4\frac{2\pi}{L}$ extrapolate near, but not exactly, to the theoretical prediction, which we attribute to smallness of the system sizes. The superimposed lines are quadratic fits over the largest few circumferences, extrapolating to give $v_\phi \approx 1.33$, $v_\chi \approx 0.21$. (Right) The theoretical placement of the energy levels for the state. Here the boson counting (1,1,2,3,5) and the Majorana counting (1,0,1,1,2) are apparent. See App. C for detailed explanation of the counting in this plot and data for other charge sectors.

to continue to higher q.

This same technique can be used for more complicated wave functions such as the Moore-Read state, as shown in Fig. 9. We extrapolate the velocities of both the charge and neutral modes to be $v_\phi \approx 1.33$ and $v_\chi \approx 0.21$ respectively. We note that the extrapolation is only possible for sufficiently large circumferences $L \gtrsim 20\ell_B$, which is well within reach using the MPS representation of the wave function.

Figure 8(b) shows that in the orbital-cut, $\tilde{E}$ does not extrapolate to the CFT linear dispersion. Rather, they appear to follow power law decays $\tilde{E}_a \sim L^{-\zeta_a}$ with different ζ_a for each state a. For example, the fit for $k = \frac{2\pi}{L}$ gives $\zeta \approx 3.0$, while $\zeta \approx 2.3$, 2.1 for the two set of states at $k = 2\frac{2\pi}{L}$. (In the real-space case, $\zeta = 1$ for all the levels.) Unfortunately, the range of data available is insufficient to draw any conclusions.

Finally, we note that one can extract the topological entanglement entropy in either types of cut. This was shown in Fig. 3 where we used both the entropy S and the zero momentum state E_0 as a function of L. For each L we perform a windowed fit; presenting the intercept of

the best line fit through the neighboring points. While it is possible to extract γ from any of the four computed quantities, we can see that the real-space cut is less oscillatory than the orbital cut. At the same time, using the orbital cut E_0 seems to give a much better convergence of γ than any of the other methods, *i.e.*, the system size L required to computed $\mathcal{D} = e^\gamma$ via the orbital E_0 to accuracy ± 0.5 is the smallest. Table I lists the entanglement velocities and TEE for various Laughlin states and the $q = 2$ MR state, as well as the velocities extracted via the method used in Figs. 8(a) and 9.

VII. CONCLUSION

We have shown how the CFT structure in model FQH wave functions enable us to represent them as matrix product states. These MPSs can be evaluated numerically on an infinite cylinder; the distinct advantages of this geometry, as well as the efficiency of the MPS, allow us to study in detail the scaling properties of the Moore-Read entanglement spectrum, including a definitive identification of the $U(1)$ and Majorana modes and their velocities.

There are several future directions. The MPS representation is well suited for studying the screening properties of the states as well as their Berry connections, so it would be valuable to numerically implement the MR quasiholes in order to verify various screening arguments.[51] As we have noted, our construction also generalizes to other topological phases whose model states can be expressed as a correlation function of a lower dimensional field theory. The resulting picture is strikingly similar to the 'entanglement renormalization' classification of 1D phases exemplified in the AKLT state. In particular, it would appear that the fixed points of the entanglement renormalization scheme may be interpreted as some form of fixed point for the auxiliary field theory when expressed as a tensor network – for topological phases, a massless fixed point, while for trivial phases, a massive fixed point. Making this connection precise would be an intriguing development.

Appendix A: Evaluation of B-matrices for Laughlin states

Here we provide more detail on the precise form of the Laughlin MPS and its numerical implementation. The mode expansion of the chiral boson is

$$\phi(w) = \sum_{n \neq 0} \frac{w^{-n}}{\sqrt{|n|}} a_n + \phi_0 + \frac{\pi_0}{i} \log(w), \qquad \text{(A1)}$$

$$[\phi_0, \pi_0] = i, \quad [a_n, a_m] = \delta_{n+m}.$$

The field is composed of the fluctuating part $\phi'(w)$ and the 'zero mode',

$$\phi(w) = \phi'(w) + \phi_0 + \frac{\pi_0}{i} \log(w). \qquad \text{(A2)}$$

The states of the fluctuating sector can be labeled by occupation numbers, which we denote by a string of positive integers P. For example, $|0\rangle$ denotes the ground state, $|221\rangle = \frac{1}{\sqrt{2}} a_2^\dagger a_2^\dagger a_1^\dagger |0\rangle$, *etc.* We define $|P|$ to be the total momentum of $|P\rangle$, given by the sum of the integers. The states of the zero-mode sector are labeled by the eigenvalues of π_0. For convenience, we define 'charge' by $\hat{N} = \sqrt{q}\pi_0$, chosen such that the electron has charge q. The states of the zero-mode sector are labeled by $|N\rangle$, so the full CFT is then spanned by $|P, N\rangle$.

Treating first the 'free' evolution U, we find

$$H = \frac{2\pi}{L}\left[|P| + \frac{1}{2q}N^2\right], \qquad \text{(A3)}$$

$$U(\delta\tau)_{P,N;P',N'} = \delta_{P,P'}\delta_{N,N'} e^{-\left(\frac{2\pi\ell_B}{L}\right)^2 \left[|P| + \frac{1}{2q}N^2\right]}. \qquad \text{(A4)}$$

Now we calculate the on-site term T, first by converting from the coherent state form $T[\psi]$ to the occupation basis, T^m:

$$T[\psi] = e^{-\frac{i}{2\sqrt{q}}\phi_0} e^{\hat{\mathcal{V}}_0 \psi} e^{-\frac{i}{2\sqrt{q}}\phi_0}$$
$$= \sum_m T^m (m!)^{3/2} \psi^m. \qquad \text{(A5)}$$

$$T^m \equiv \frac{1}{\sqrt{m!}} e^{-\frac{i}{2\sqrt{q}}\phi_0} \left(\hat{\mathcal{V}}_0\right)^m e^{-\frac{i}{2\sqrt{q}}\phi_0}. \qquad \text{(A6)}$$

We next compute the matrix elements of the vertex operator,

$$\langle P, N|\hat{\mathcal{V}}_0|P', N'\rangle$$
$$= \langle P, N|e^{i\sqrt{q}\phi'(w) + i\sqrt{q}\phi_0 + N\log(w)]}|P', N'\rangle. \qquad \text{(A7)}$$

The zero-mode part depends only on N,

$$\langle N|e^{i\sqrt{q}\phi_0 + \hat{N}\log(w)}|N'\rangle = \delta_{N-N',q} w^{N+N'/2}. \qquad \text{(A8)}$$

The fluctuating part depends only on the oscillators $|P\rangle$, so we define

$$A^n_{P,P'} = \langle P|\oint \frac{dw}{2\pi i} w^{-n-1} e^{i\sqrt{q}\phi'(w)}|P'\rangle. \qquad \text{(A9)}$$

Hence A^n is simply the nth coefficient of a Taylor expansion in w. The matrices A are non-zero only for $P - P' = -(N + N')/2$, due to momentum conservation. Numerically, we impose a cutoff Λ such that we only keep states $|P\rangle$ with $|P| \leq \Lambda$, which allows us to evaluate A for only a finite number of states. The time to compute A is proportional to its number of entries, so the construction of the MPS is an insignificant part of the computational cost (*i.e.*, compared to matrix multiplication). Combining the zero-mode and fluctuations,

$$\langle P, N|\hat{\mathcal{V}}_0|P', N'\rangle = A^{-\frac{N+N'}{2}}_{PP'} \delta_{N-N',q}. \qquad \text{(A10)}$$

Finally, the sandwiching background charge contributes $e^{-\frac{i}{\sqrt{q}}\phi_0} = \delta_{P,P'}\delta_{N-N',-1}$ to each site.

Focusing on the case of fermions where there is at most one particle per orbital,

$$T^0_{P,N;P',N'} = \delta_{P,P'}\delta_{N-N',-1} \qquad \text{(unoccupied)}, \qquad \text{(A11a)}$$

$$T^1_{P,N;P',N'} = A^{-\frac{N+N'}{2}}_{PP'} \delta_{N-N',q-1} \qquad \text{(occupied)}. \qquad \text{(A11b)}$$

For case of bosons, the higher occupation states involve products of the A's.

The q fold ground state degeneracy of the Laughlin states can be seen by noting that on a particular bond, $e^{2\pi i N/q}$ is a constant, and can be chosen to take q values. In the small L limit, these q states evolve into the 'thin torus' wave functions[41] in which we keep only the $|P| = 0$ states of the CFT.

Appendix B: Evaluation of B-matrices for Moore-Read state

The CFT associated with the Moore-Read state is a tensor product of a chiral boson ϕ and a Majorana mode χ. We first give a brief review of the structure of the chiral Majorana CFT on a cylinder.[52] The states form four sectors according to their boundary condition (bc), (periodic '**P**' or antiperiodic '**AP**') and number parity (even '+1' or odd '−1'). We denote the lowest energy states of these four sectors by '$|\mathbb{1}\rangle$' for **AP**/1, '$|\chi\rangle$' for **AP**/−1, '$|\sigma\rangle$' for **P**/1 and '$|\mu\rangle$' for **P**/−1. In the periodic sector the Majorana has modes $\chi_n : n \in \mathbb{Z}$, while in the anti-periodic sector it has modes $\chi_m : m \in \mathbb{Z} + \frac{1}{2}$. The states of the **P**/**AP** sectors can be obtained by acting with the **P**/**AP** modes χ_{-m} on $|\sigma\rangle/|\mathbb{1}\rangle$ respectively. Within a given sector, the states can then be labeled by a string of numbers P_χ; they are either integers or half-integers depending on the bc, and do not repeat because of the fermionic statistics. Letting $|P_\chi|$ denote the total momentum of the Majorana,

$$H_\chi = \frac{2\pi}{L}[|P_\chi| + \Delta] \qquad \text{(B1)}$$

where $\Delta = \{0, \frac{1}{16}\}$ for the **AP** and **P** sectors respectively, though Δ can be ignored as it only changes the normalization of the state.

For simplicity we consider the case in which the physical particles are fermions, which we take to have periodic boundary conditions. The operator $e^{i\sqrt{q}\phi(z)}\chi(z)$ must be periodic in z at the location of the Landau orbitals τ_n (our choice of gauge has a twist boundary condition in between). This introduces a constraint between the zero mode of the boson, $\hat{N} = \sqrt{q}\hat{\pi}_0$, and the boundary condition of the Majorana: for **P**, we must have $N \in \mathbb{Z}$, while for **AP**, we must have $N \in \mathbb{Z} + \frac{1}{2}$. The boundary conditions will correspond to different degenerate ground states, with 4 states of type **AP** and 2 of type **P**, for a total of 6 on the infinite cylinder (for a torus, the **P** sector acquires an additional 2 states depending on the parity of the electron number).[53]

The total energy of the combined CFT is

$$H = \frac{2\pi}{L}\left[|P_\chi| + |P_\phi| + \frac{1}{2q}N^2\right] \quad \text{(B2)}$$

with $|P_\phi|$ and N arising for the boson. As for the Laughlin state, $U = e^{-\delta\tau H}$ is diagonal if we work in the occupation basis. Constructing the T matrices proceeds as for the Laughlin case, but we must include the Majorana sector in the computation of $\hat{\mathcal{V}}_0 = \oint \frac{dw}{2\pi i}w^{-1}\chi(w)e^{i\sqrt{q}\phi(w)}$. Letting

$$\chi^m_{P_\chi, P'_\chi} = \langle P_\chi|\chi_m|P'_\chi\rangle \quad \text{(B3)}$$

denote the matrix elements of the Majorana operators, the required matrix element is

$$\langle P_\phi, P_\chi, N|\hat{\mathcal{V}}_0|P'_\phi, P'_\chi, N'\rangle$$
$$= \sum_m \chi^{-m}_{P_\chi, P'_\chi} A^{m-\frac{N+N'}{2}}_{P_\phi, P'_\phi} \delta_{N-N',q}, \quad \text{(B4)}$$

with A defined as for the Laughlin case.

For fermions, where there is at most one particle per orbital,

$$T^0_{(P_\phi, P_\chi, N),(P', P'_\chi, N')} \quad \text{(B5a)}$$
$$= \delta_{P_\phi, P'_\phi}\delta_{P_\chi, P'_\chi}\delta_{N-N',-1} \quad \text{(unoccupied)},$$

$$T^1_{(P_\phi, P_\chi, N),(P', P'_\chi, N')} \quad \text{(B5b)}$$
$$= \sum_m \chi^{-m}_{P_\chi, P'_\chi} A^{m-\frac{N+N'}{2}}_{P_\phi, P'_\phi} \delta_{N-N',q-1} \quad \text{(occupied)}.$$

For the case of bosons, the higher occupation states involve products of the $\mathcal{V}_0$'s.

The $3q$ fold ground state degeneracy of the MR states can be seen by first choosing a bc sector, **P** or **AP**. In the **AP** sector, $(-1)^F e^{i\pi N/q}$ is a constant (where F is the Majorana number), which takes $2q$ values, each leading to a distinct state. It is also constant in the **P** sector, but here the $2q$ values only lead to q distinct states. This is because inserting the Majorana zero-mode χ_0 somewhere
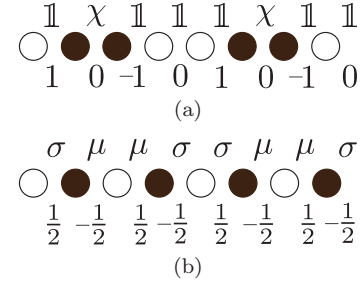

FIG. 10. The thin torus orbital wave functions for the (a) antiperiodic and (b) periodic sectors. Each site corresponds to an orbital, which is either filled (black) or empty (white). Each bond has only a single state of the CFT, which we decompose into the Majorana part, shown above the bond, and zero mode of the boson N, shown below the bond.

in the chain changes the CFT labels we assign to the Schmidt vectors, but does not actually change the physical state. In the small L limit, these $3q$ states evolve into 'thin torus' wave functions.[42] In this limit, we restrict the Majorana CFT to the states $\{|\mathbb{1}\rangle, |\chi\rangle, |\sigma\rangle, |\mu\rangle\}$, and fix $|P_\phi| = 0$ for the boson – the 8 resulting states are precisely the 'highest weight' states of the CFT, as illustrated in Fig. 10.

Appendix C: The counting of the Moore-Read state

As explained in the last section, the chiral Majorana CFT may be separated into four sectors, by periodicity of the boundary as well as the particle number parity.

In the periodic sectors σ and μ, the excitations have momenta which are integral multiples of $\Delta k = \frac{2\pi}{L}$, hence the counting of level n is the number of partitions of n into an even/odd number of distinct non-negative integers. The number of states at momenta $0, \Delta k, 2\Delta k, ...$ are as follows,[54]

$$\mu, \sigma: \quad 1, 1, 1, 2, 2, 3, 4, 5, 6, 8, 10, 12, 15, 18, ... \quad \text{(C1a)}$$

(Because the presence of the zero-momentum mode, the counting of the two **P** sectors are identical.)

In the antiperiodic sectors the excitations have momenta which are integer-plus-half multiples of Δk, or in other words, twice the momentum is always an odd multiple of Δk. Hence in the $\mathbb{1}$ sector the counting of level n is given by the partitions of $2n$ into positive odd integers.[55]

$$\mathbb{1}: \quad 1, 0, 1, 1, 2, 2, 3, 3, 5, 5, 7, 8, 11, 12, ... \quad \text{(C1b)}$$

The same definition also hold for the χ sector, with counting as follows,[56]

$$\chi: \quad 1, 1, 1, 1, 2, 2, 3, 4, 5, 6, 8, 9, 12, ... \quad \text{(C1c)}$$

Note that since there are an odd number of excitations, the lowest energy state is $|\chi\rangle = \chi_{1/2}|\mathbb{1}\rangle$ with momentum
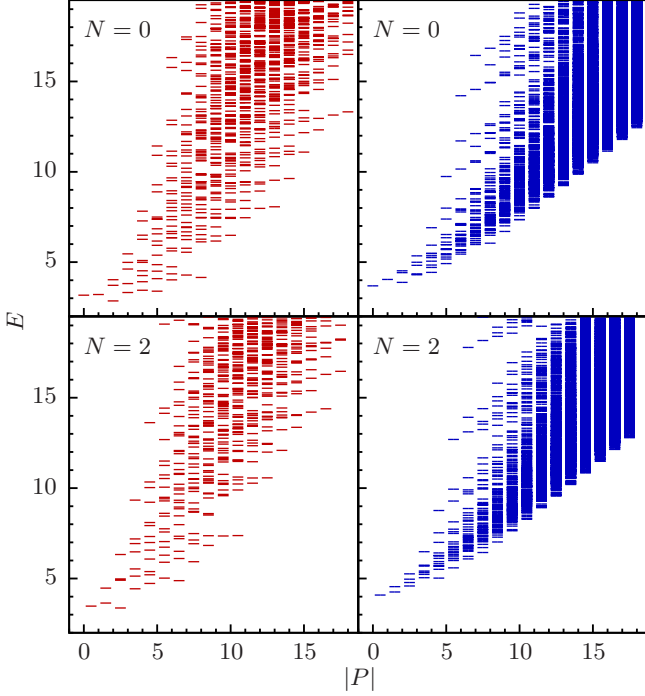
FIG. 11. The entanglement spectra of the $q = 2$ Moore-Read state at $L = 25\ell_B$, with the orbital (left) and real-space (right) cut, in the $N = 0$ (top) and $N = 2$ (bottom) charge sectors. In the orbital case, the cut takes place on the bond with $|\mathbb{1}\rangle$ Majorana and $N = 0$ boson state in the thin torus limit (cf. Fig. 10). The real-space cut takes place at the τ centered on that bond. For $N = 0$, the counting of the states are 1, 1, 3, 5, 10, 16, etc, while for $N = 2$, the counting are 1, 2, 4, 7, 13, etc.

$\frac{1}{2}\Delta k$. The counting in this sector corresponds to the number of states at momenta $\frac{1}{2}\Delta k, \frac{3}{2}\Delta k, \frac{5}{2}\Delta k, ...$.

Combined with the chiral boson, the counting of the Moore-Read edge spectra are[57][58]

$$\mathbb{1}: \qquad 1, 1, 3, 5, 10, 16, 28, 43, 70, ... , \qquad \text{(C2a)}$$
$$\chi: \qquad 1, 2, 4, 7, 13, 21, 35, 55, 86, ... , \qquad \text{(C2b)}$$
$$\mu, \sigma: \qquad 1, 2, 4, 8, 14, 24, 40, 64, 100, ... \qquad \text{(C2c)}$$

(Again, in the χ sector, the momenta are shifted by $\frac{1}{2}\Delta k$.) Figure 11 shows the orbital and real-space cut of the $q = 2$ MR state giving the $\mathbb{1}$ sector.

Notice that in the **AP** case, the Majorana sector alternates between $\mathbb{1}$ and χ sectors whenever an orbital is filled (see Fig. 10). Hence the entanglement spectrum with different charges would also alternate between the countings (C2a) and (C2b), shown clearly in Fig. 11. Figure 12 shows the relative entanglement energies of $q = 2$ MR state at the $N = \pm q$ charge sectors, contrast this to the $N = 0$ sector of Fig. 9.
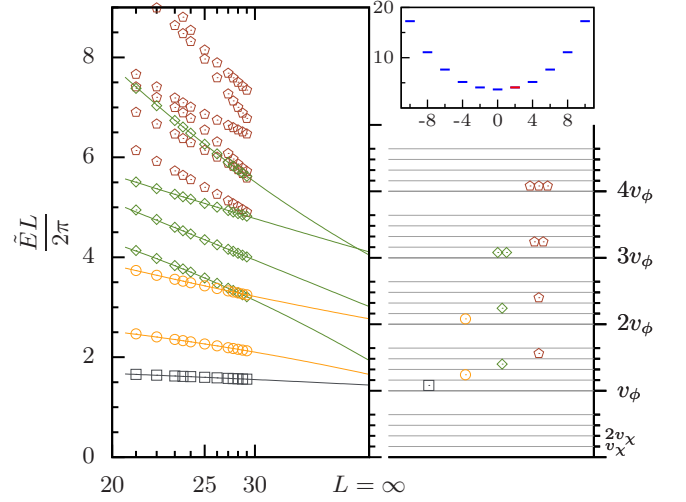

FIG. 12. Extrapolating the entanglement energies $\tilde{E}L/2\pi$ for the Moore-Read state at $\nu = 1/2$. The real-space cut is physically centered on the bond with $\mathbb{1}$ sector (in the thin torus limit), but the data is shown in the $N = 2$ charge sector, and hence the counting matches that of the χ sector.

(Left) The energy states at momenta $\frac{\pi}{L}, 3\frac{\pi}{L}, 5\frac{\pi}{L}, 7\frac{\pi}{L}$ are labeled by their shape, with their values extrapolated to $L = \infty$. (Right) The theoretical energy levels of the MR state for the χ sector. (Upper right inset) The least-momentum state in each charge sector N at $L = 25\ell_B$, with the sector of interest marked red.

The lowest states extrapolates to $v_\phi + \frac{1}{2}v_\chi$, consistent with Eq. (42) (using $\Delta_{\phi h} = \frac{N^2}{2q} = 1$). (States with momenta $7\frac{\pi}{L}$ do not extrapolate to their theoretical values due to insufficient system sizes.) Contrast this plot to the $N = 0$ sector of Fig. 9.

Appendix D: Evaluation of $\mathcal{Q}$-matrices for Laughlin and Moore-Read quasiholes

Evaluation of the Q-matrices for the Laughlin state can be done in a similar manner to the bulk B-matrices, but omitting the contour integration:

$$Q_{P,N;P',N'} = \delta_{N-N',1} (sw)^{N+N'/2q} \langle P|e^{i\phi'(w)/\sqrt{q}}|P'\rangle \qquad \text{(D1)}$$

where $w = e^{-\frac{2\pi i}{L}\eta_x}$ and $s = \pm 1$ for bosons or fermions respectively. Note that the momentum is no longer conserved.

The Moore-Read case is more complex. In the context of the Majorana CFT, the Ising order and disorder fields σ, μ are 'twist' fields, interpolating between **AP** and **P** periodic bc's. We take the point of view that the fields σ and μ have fixed fermion parity $+1$ and -1 respectively. The resulting fusion rules are

$$[\sigma][\sigma] = [\mu][\mu] = [\chi][\chi] = [\mathbb{1}], \qquad \text{(D2)}$$
$$[\mu][\sigma] = \mathbb{1}, \ [\mu][\chi] = [\sigma], \ [\sigma][\chi] = [\mu]. \qquad \text{(D3)}$$

In this approach, there are *two* possible quasihole insertions, $\sigma(\eta)e^{i\phi/\sqrt{q}}$, and $\mu(\eta)e^{i\phi/\sqrt{q}}$. As $\chi_0\sigma \sim \mu$, this is a direct realization of the picture in which each vortex has a Majorana zero-mode. The non-trivial vector space of quasihole excitations arises from the freedom of choosing σ or μ, subject to the constraint that they fuse properly to the vacuum.

Fortunately the techniques for evaluating matrix elements of the type

$$\sigma_{P_\chi,P'_\chi} = \langle P_\chi|\sigma(0)|P'_\chi\rangle \tag{D4}$$

have already been developed in the 'truncated-fermionic-space-approach' to the perturbed Ising CFT.[59]

Consider, for example, the **AP** to **P** case. Arbitrary states can be built by acting with the modes χ_{-n}, so without loss of generality we consider the matrix element

$$\langle\sigma|\prod_{\{m_i\in P_\chi\}}\chi_{m_i}\sigma(\eta)\prod_{\{n_i\in P'_\chi\}}\chi_{-n_i}|\mathbb{1}\rangle. \tag{D5}$$

The chief technical result of Ref. 59 Eqs. 2.9-2.13 is that there exists an easily computed matrix $C(\eta)$ such that

$$\langle\sigma|\cdots\chi_m\sigma(\eta)\cdots|\mathbb{1}\rangle = \langle\sigma|\cdots\sigma(\eta)C_{mn}(\eta)\chi_n\cdots|\mathbb{1}\rangle. \tag{D6}$$

After commuting all χ across the insertion, the Majoranas are brought to normal ordered form, reducing the problem to Wick contractions and the matrix elements

$$\langle\sigma|\sigma|\mathbb{1}\rangle = C_{\sigma\sigma1} = 1, \tag{D7}$$
$$\langle\sigma|\mu|\chi\rangle = C_{\sigma\mu\chi} = 1, \quad etc. \tag{D8}$$

We have not as of yet implement the MR quasiholes numerically, which would be a worthwhile check given the subtleties of this case.

[1] X.-G. Wen, Adv. Phys. **44**, 405 (1995).
[2] A. Kitaev and J. Preskill, Phys. Rev. Lett. **96**, 110404 (2006).
[3] M. Levin and X.-G. Wen, Phys. Rev. Lett. **96**, 110405 (2006).
[4] M. Aguado and G. Vidal, Phys. Rev. Lett. **100**, 070404 (2008).
[5] H. Li and F. D. M. Haldane, Phys. Rev. Lett. **101**, 010504 (2008).
[6] X.-L. Qi, H. Katsura, and A. W. W. Ludwig, Phys. Rev. Lett. **108**, 196402 (2012).
[7] R. B. Laughlin, Phys. Rev. Lett. **50**, 1395 (1983).
[8] G. Moore and N. Read, Nuclear Physics B **360**, 362 (1991).
[9] M. Fannes, B. Nachtergaele, and R. Werner, Communications in Mathematical Physics **144**, 443 (1992).
[10] F. Verstraete and J. Cirac, "Renormalization algorithms for Quantum-Many Body Systems in two and higher dimensions," (2004), arXiv:cond-mat/0407066.
[11] S. R. White, Phys. Rev. Lett. **69**, 2863 (1992).
[12] S. Östlund and S. Rommer, Phys. Rev. Lett. **75**, 3537 (1995).
[13] D. Perez-Garcia, F. Verstraete, M. M. Wolf, and J. I. Cirac, Quantum Info. Comput. **7**, 401 (2007).
[14] L. Fidkowski and A. Kitaev, Phys. Rev. B **83**, 075103 (2011).
[15] A. M. Turner, F. Pollmann, and E. Berg, Phys. Rev. B **83**, 075102 (2011).
[16] X. Chen, Z.-C. Gu, and X.-G. Wen, Phys. Rev. B **83**, 035107 (2011).
[17] N. Schuch, D. Pérez-García, and I. Cirac, Phys. Rev. B **84**, 165139 (2011).
[18] F. Verstraete, J. I. Cirac, J. I. Latorre, E. Rico, and M. M. Wolf, Phys. Rev. Lett. **94**, 140601 (2005).
[19] I. Affleck, T. Kennedy, E. H. Lieb, and H. Tasaki, Phys. Rev. Lett. **59**, 799 (1987).
[20] F. D. M. Haldane, Phys. Rev. Lett. **50**, 1153 (1983).
[21] D. P. Arovas, A. Auerbach, and F. D. M. Haldane, Phys. Rev. Lett. **60**, 531 (1988).
[22] A. M. Läuchli, E. J. Bergholtz, J. Suorsa, and M. Haque, Phys. Rev. Lett. **104**, 156404 (2010).
[23] A. M. Läuchli, E. J. Bergholtz, and M. Haque, New Journal of Physics **12**, 075004 (2010).
[24] Z. Liu, E. J. Bergholtz, H. Fan, and A. M. Läuchli, Phys. Rev. B **85**, 045119 (2012).
[25] M. Haque, O. Zozulya, and K. Schoutens, Phys. Rev. Lett. **98**, 060401 (2007).
[26] O. S. Zozulya, M. Haque, K. Schoutens, and E. H. Rezayi, Phys. Rev. B **76**, 125310 (2007).
[27] R. Thomale, A. Sterdyniak, N. Regnault, and B. A. Bernevig, Phys. Rev. Lett. **104**, 180502 (2010).
[28] A. Sterdyniak, A. Chandran, N. Regnault, B. A. Bernevig, and P. Bonderson, Phys. Rev. B **85**, 125308 (2012).
[29] J. Dubail, N. Read, and E. Rezayi, Phys. Rev. B **85**, 115321 (2012).
[30] S. Iblisdir, J. I. Latorre, and R. Orús, Phys. Rev. Lett. **98**, 060402 (2007).
[31] J. Dubail, N. Read, and R. E. H., "Edge state inner products and real-space entanglement spectrum of trial quantum Hall states," (2012), unpublished, arXiv:1207.7119.
[32] R. Shankar and A. Vishwanath, Phys. Rev. Lett. **107**, 106803 (2011).
[33] A. Y. Kitaev, Ann. Phys. (NY) **303**, 2 (2003).
[34] J. Dubail and N. Read, Phys. Rev. Lett. **107**, 157001 (2011).
[35] J. I. Cirac, D. Poilblanc, N. Schuch, and F. Verstraete, Phys. Rev. B **83**, 245134 (2011).
[36] F. Verstraete and J. I. Cirac, Phys. Rev. Lett. **104**, 190405 (2010).
[37] V. P. Yurov and A. B. Zamolodchikov, International Journal of Modern Physics A **05**, 3221 (1990).
[38] X.-G. Wen, International Journal of Modern Physics B **06**, 1711 (1992).
[39] P. Fendley, M. Fisher, and C. Nayak, Journal of Statistical

Physics **126**, 1111 (2007).

[40] Y. Zhang, T. Grover, A. Turner, M. Oshikawa, and A. Vishwanath, Phys. Rev. B **85**, 235151 (2012).

[41] R. Tao and D. J. Thouless, Phys. Rev. B **28**, 1142 (1983).

[42] E. J. Bergholtz, J. Kailasvuori, E. Wikberg, T. H. Hansson, and A. Karlhede, Phys. Rev. B **74**, 081308 (2006).

[43] M. Nakamura, Z.-Y. Wang, and E. J. Bergholtz, Phys. Rev. Lett. **109**, 016401 (2012).

[44] J. L. Cardy, Nuclear Physics B **275**, 200 (1986).

[45] T. H. Hansson, M. Hermanns, and S. Viefers, Phys. Rev. B **80**, 165330 (2009).

[46] D. Arovas, J. R. Schrieffer, and F. Wilczek, Phys. Rev. Lett. **53**, 722 (1984).

[47] A. M. Turner, Y. Zhang, and A. Vishwanath, Phys. Rev. B **82**, 241102 (2010).

[48] I. D. Rodríguez and G. Sierra, Phys. Rev. B **80**, 153303 (2009).

[49] I. D. Rodríguez, S. H. Simon, and J. K. Slingerland, Phys. Rev. Lett. **108**, 256806 (2012).

[50] G. Vidal, Phys. Rev. Lett. **98**, 070201 (2007).

[51] P. Bonderson, V. Gurarie, and C. Nayak, Phys. Rev. B **83**, 075303 (2011).

[52] P. H. Ginsparg, "Applied Conformal Field Theory," (1988), arXiv:hep-th/9108028.

[53] N. Read and D. Green, Phys. Rev. B **61**, 10267 (2000).

[54] The sequence (C1a) is given at oeis.org/A000009.

[55] The fact that we require an even number of integers in the partition is automatically enforced. The sequence (C1b) is given at oeis.org/A069910.

[56] The sequence (C1c) is given at oeis.org/A069911 respectively.

[57] X.-G. Wen, Phys. Rev. Lett. **70**, 355 (1993).

[58] The sequence (C2c) is given at oeis.org/A015128. The sequences (C2a) and (C2b) interlaced together is given at oeis.org/A006950.

[59] V. P. Yurov and A. B. Zamolodchikov, International Journal of Modern Physics A **06**, 4557 (1991).